

Error Estimation for Single-Image Human Body Mesh Reconstruction

Hamoon Jafarian
Ontario Tech University
Oshawa, Ontario, Canada

hamoon.jafarian@ontariotechu.ca

Faisal Z. Qureshi
Ontario Tech University
Oshawa, Ontario, Canada

faisal.qureshi@ontariotechu.ca

Abstract

Human pose and shape estimation methods continue to suffer in situations where one or more parts of the body are occluded. More importantly, these methods cannot express when their predicted pose is incorrect. This has serious consequences when these methods are used in human-robot interaction scenarios, where we need methods that can evaluate their predictions and flag situations where they might be wrong. This work studies this problem. We propose a method that combines information from OpenPose and SPIN—two popular human pose and shape estimation methods—to highlight regions on the predicted mesh that are least reliable. We have evaluated the proposed approach on 3DPW, 3DOH, and Human3.6M datasets, and the results demonstrate our model’s effectiveness in identifying inaccurate regions of the human body mesh. Our code is available at <https://github.com/Hamoon1987/meshConfidence>.

1. Introduction

The applications of Human Body Mesh Recovery (HMR) are diverse and numerous. HMR, for example, is useful for Human-Robot Interaction (HRI) scenarios, where accurate 3D mesh representation is essential for ensuring safe interactions [18]. Drones, self-driving cars, and human-robot collaborative manufacturing systems are some examples where a three-dimensional understanding of the environment and humans is critical for reliable operation [16]. Additionally, the animation and movie industries can benefit significantly from HMR by simplifying the process of character motion capture (MOCAP) and reducing the costs involved [26]. Other areas such as part and foreground segmentation, computer-assisted coaching, and virtual try-on can also leverage the capabilities of 3D mesh recovery to enhance their outcomes [25].

The task of estimating a human body mesh from a single

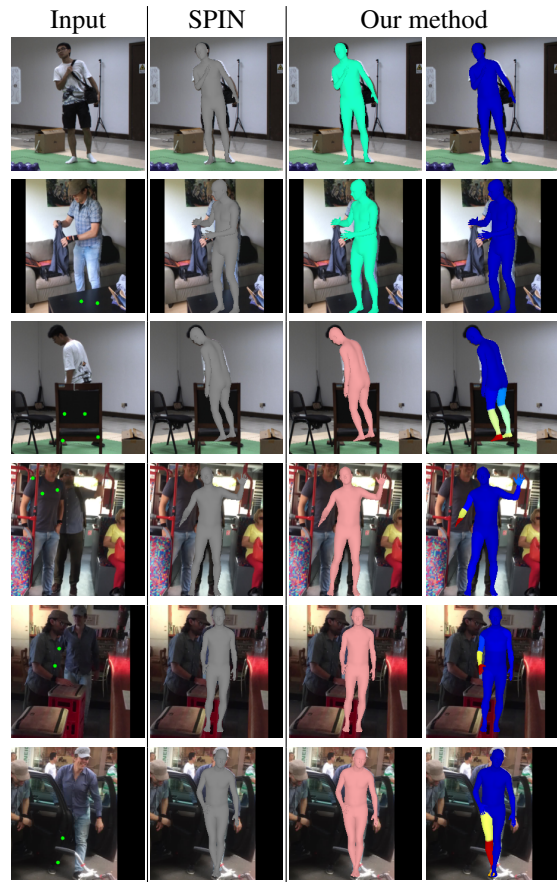


Figure 1: Human body mesh recovery using the SPIN model vs. our method. The input images are in the first column; the recovered meshes using SPIN are shown in the second column. Our method identifies whether or not the recovered mesh corresponds to a partially occluded human and highlights regions of the mesh that are unreliable since these represent parts of the human body that are not visible in the image.

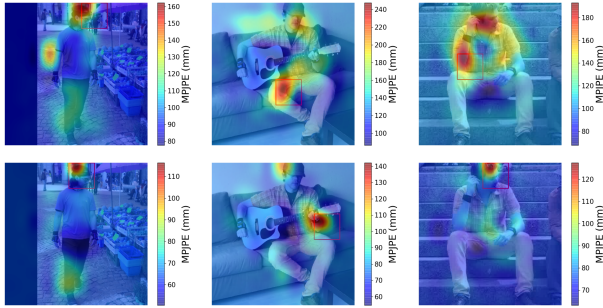


Figure 2: Pixel Locations based Occlusion Sensitivity Analysis. A 40×40 square (gray) occluder is moved across the image and MPJPE values are computed (for each) for SPIN (top-row) and OpenPose (bottom-row) models. The heatmaps highlight locations in the image that strongly affects the performance of the two models. Both models are sensitive to occlusions in regions shown in red. Image size is 224×224 and the stride is selected to be 20.

RGB image is an active area of research that has garnered significant interest in the field of computer vision. Koltoures and colleagues [13] proposed SPIN that achieves impressive results on single image human body mesh recovery. SPIN represents a significant improvement in human pose and shape estimation over prior methods, and it is now a widely adopted baseline in the field. A number of recent methods attempt to recover human body mesh in the presence of occlusions [31, 12, 11]. None of these methods, however, provide a confidence score for the recovered mesh. The ability to tell whether or not the recovered mesh is correct or to identify parts of the mesh that may be inaccurate is particularly relevant for human-robot interaction scenarios. A robot, for example, can choose to halt its operation if it deems that the recovered mesh is not reliable. Alternatively a robot may adjust its viewpoint to achieve a better reconstruction if it identifies one or more parts of the mesh to be unreliable.

Here we tackle the problem of estimating the error in the reconstructed human body meshes. We propose a method that fuses information from SPIN and OpenPose [2] to highlight regions of the recovered mesh that *may* be inaccurate (Figure 1). OpenPose estimates human joints’ keypoints, and it is able to identify joints that are not visible in the image. The proposed method leverages the observation that SPIN and OpenPose agree when the person is visible in the image; whereas, these two methods disagree when the person is partially occluded. We have used *sensitivity analysis* to quantify the disagreement between SPIN and OpenPose models under occluded settings. The differences between the joints’ keypoints estimated by OpenPose and those constructed by projecting the human body mesh recovered by SPIN are fed into two multi-layer perceptron networks to

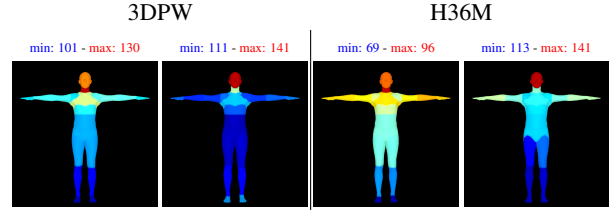


Figure 3: Joints based Occlusion Sensitivity Analysis. For every image in 3DPW and H36M datasets, a square occluder is pasted over each joint in turn and MPJPE values are computed for SPIN (left) and OpenPose (right) models. MPJPE errors for each joint are visualized by highlighting the vertices (of the mesh) that correspond to each joint. The figures depict model performance if one of the joints is occluded. This figure is best viewed in color.

compute an error estimate for each region of the mesh. In Figure 1 (last column from right) regions shown in red depict mesh parts with the lowest reliability. Note that these regions correspond to the parts of the human body that are not visible in the image.

To the best of our knowledge, this work represents the first attempt at estimating error in single-image 3D human body mesh reconstructions. The contributions of the work presented here are: 1) location-based and joint-based occlusion sensitivity analysis to quantify the relationship between the disagreement of OpenPose and SPIN joint location estimates and the “true” error; 2) a mesh classifier that identifies whether or not the recovered mesh is reliable; and 3) a worst joint classifier that selects the least reliable joint. This work represents a significant step towards improving the safety and reliability of those human-robot interactions that rely upon accurate reconstructions of human body mesh by providing additional information about the confidence and reliability of the estimated mesh.

2. Related Work

2D Keypoint Estimation. 2D keypoint estimation aims to localize body joints within an image. Joints’ keypoint estimation comes in two flavours: regression-based methods [24, 17, 30] and detection-based methods [23, 3]. Top-down approaches achieve better accuracy in multi-person scenarios; however, bottom-up approaches are often faster and are better suited for real-world applications that demand real-time performance [5]. Pishchegulin et al. [21] proposed DeepCut, a CNN-based body part detector, and Insafutdinov et al. [7] improved the DeepCut model by employing a ResNet-based deep part detector. Cao et al. [2] introduced Part Affinity Fields (PAFs) that encode the position and orientation of human body parts and propose OpenPose, an accurate, fast, and robust model for multi-person

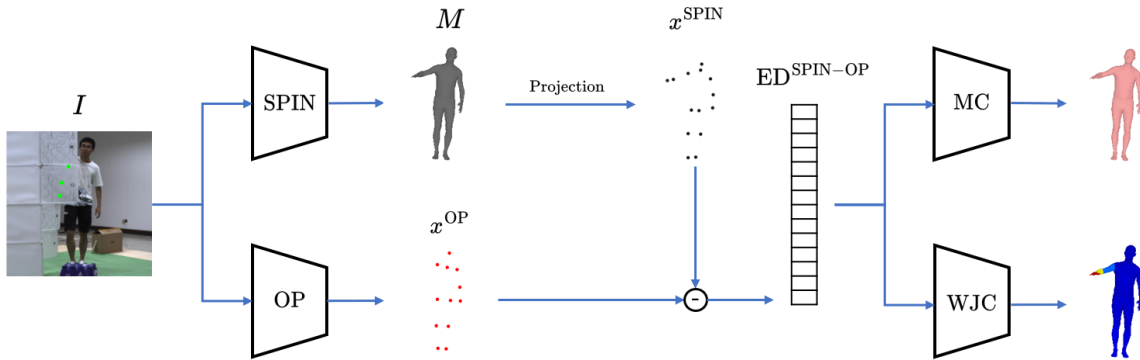


Figure 4: Overview of the Proposed Framework. The input image I is passed through the SPIN and OpenPose models. Then, the estimated SPIN mesh (M) is regressed and projected into 2D joint coordinates. Comparing the results with the OpenPose predicted 2D joint positions, Estimation Difference (ED) is obtained. Afterward, ED is employed to train the Mesh Classifier (MC) and Worst Joint Classifier (WJC) that decide the SPIN mesh quality and detect the least reliable parts of the mesh, respectively.

joints’ keypoints estimation.

3D Pose and Shape Estimation. Broadly speaking 3D pose and shape estimation methods are divided into two classes: optimization-based methods that deform a canonical pose to match the image [1, 28, 14] and regression-based methods that directly estimate the mesh from the image [9, 19, 20]. Optimization-based methods achieve good results; however, these are slow and require careful initialization. The regression-based methods, on the other hand, are difficult to train to achieve high-quality meshes [25]. Kolotoures et al. [13] proposed SPIN method for human body mesh reconstruction that employs optimization to provide explicit 3D supervision to train a regressor to construct high-quality meshes. Hybrid models achieve state-of-the-art performance. These benefit from the 3D pose and shape estimation models’ ability to capture the realistic body structure and combine it with the higher accuracy of keypoint estimation models [15].

Occlusion Handling. Inspired by random erasing [32] and synthetic occlusion [4] techniques exploited in classification and object detection tasks, some researchers suggest that data augmentation could be a suitable solution against occlusion. In this scenario, the images are occluded throughout the training process, and the model is taught to perform better against occlusion [22, 10]. Others modified the model architecture to improve the model’s robustness against occlusion. Zhang et al. [31] uses a partial UV map model to convert the occluded human body to an image inpainting problem. Georgakis et al. [6] develop a prior-informed regressor that knows the hierarchical structure of the human body, and the experiments show that this method improves the model performance against occluded cases. Kocabas et al. [12] implemented the soft attention mechanism for the HMR problem, resulting in a considerable im-

provement of the model’s robustness against occlusion. The developed part attention regressor (PARE) learns to rely on visible body parts to reason about the occluded parts.

3. Occlusion Sensitivity Analysis

We experiment with two approaches to visualize and understand the effects of partial occlusions of the human body on the performance of SPIN and OpenPose models. The first approach captures the sensitivity (of both methods) to occluded regions for a given image. The second approach, on the other hand, shows the sensitivity to an occluded joint over the entire dataset.

The first approach is inspired by [29, 12], where a square occluder is pasted onto different pixel locations in the image. Both the size and the stride of the occluder can be changed. Similar to [29], we use a grey colored square. The occluded images are passed to SPIN and OpenPose models and the errors are recorded. The performance of both models is measured using the Mean per Joint Position Error (MPJPE) that is defined as the mean value of the Euclidean distance between the ground truth and the predicted locations of all the joints. SPIN model recovers an SMPL mesh M . Using a pre-trained regressor W , it is possible to estimate 3D joint locations $X = WM$, where $X \in \mathbb{R}^{K \times 3}$. $K = 14$ refers to the number of joints. MPJPE for SPIN model is

$$\text{MPJPE}_{(m,n)}^{\text{SPIN}} = \text{Mean}_k \|X_{(m,n)} - X^{\text{gt}}\|. \quad (1)$$

Here $X_{(m,n)}$ denotes 3D joint locations when occluder is centered at location (m, n) . X^{gt} denotes ground truth 3D joint locations. For the OpenPose model, which estimates

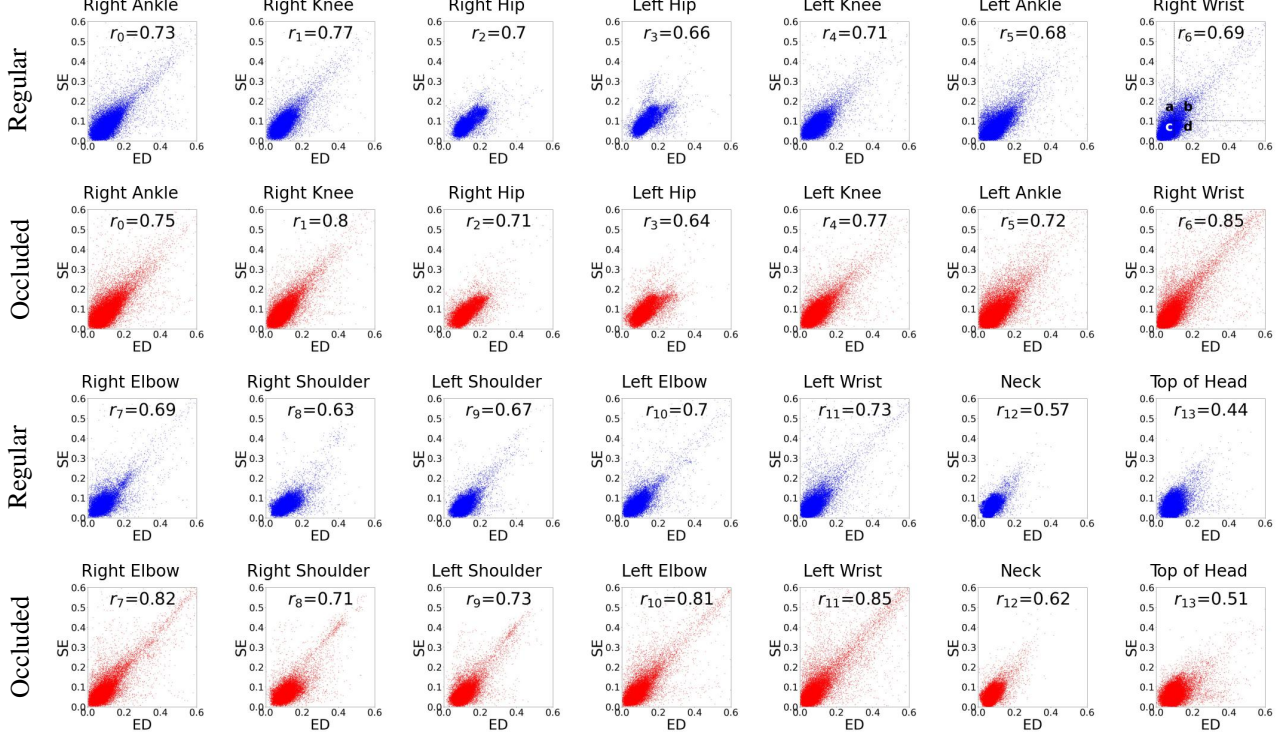


Figure 5: Pearson Correlation Coefficient. We calculate the correlation coefficient for each joint throughout the 3DPW dataset. The average value in the absence of occlusions is $\bar{r} = 0.67$. This value jumps to 0.735 for the occluded version of the 3DPW dataset. These values suggest a positive correlation between ED and SE. Four regions (a, b, c and d) are indicated in the top-right plot. Region a denotes False Positive scenarios, i.e., the estimated joint location is inaccurate, however, the proposed model has failed to identify it. Region d denotes False Negative scenarios where the estimated joint location is erroneously labelled inaccurate. Combining information from multiple joints helps deal with these scenarios.

2D joint locations $x \in \mathbb{R}^{K \times 2}$,

$$\text{MPJPE}_{(m,n)}^{\text{OP}} = \text{Mean}_k \|x_{(m,n)} - x^{\text{gt}}\|, \quad (2)$$

where $x_{(m,n)}$ and x^{gt} are 2d joint estimates when occluder is centered at (m, n) and ground truth 2d locations, respectively. Figure 2 plots MPJPE scores for both models using a heatmap. The figure shows how partial occlusions affect the performance of the two methods as measured by MPJPE.

For the second approach, the square occluder is used to hide specific joints through the entire dataset. Where as the first approach captures the occlusions sensitivity to particular image locations, the second approach finds occlusions sensitivity to different joints. In this case

$$\text{MPJPE}_k^{\text{SPIN}} = \text{Mean}_i \text{Mean}_k \|X_{i,k} - X_i^{\text{gt}}\|, \quad (3)$$

where i indices over images, k indices over images, $X_{i,k}$ denotes 3D joints' locations estimations for image i when occluder is centered on joint k . X_i^{gt} is ground truth 3D joint locations for image i . Similarly,

$$\text{MPJPE}_k^{\text{OP}} = \text{Mean}_i \text{Mean}_k \|x_{i,k} - x_i^{\text{gt}}\|. \quad (4)$$

Here $x_{i,k}$ refers to OpenPose joint estimates for image i when the occluder is centered at joint k and x_i^{gt} denotes ground truth 2D joints for image i . Figure 3 visualizes MPJPE values for both methods on an SMPL mesh. Every vertex of a joint is associated with one or more joints, and each vertex is assigned a color using MPJPE_k values, where k belongs to the set of joints associated with this vertex. These colors visualize the sensitivity of the two methods to an occluded joint.

4. Method

Figure 4 illustrates the proposed method for assigning an error estimate to different regions of the reconstructed human body mesh. It comprises three steps: 1) SPIN model is used to estimate “2D” joint locations, 2) OpenPose model is used to recover 2D joint locations, 3) The difference between the 2D joint estimates for SPIN and OpenPose is used to assign a confidence score to the mesh. When SPIN and OpenPose models correctly estimate a joint position, the estimated coordinates are close to each other and adjacent to the ground truth. However, based on the sensitivity analysis,

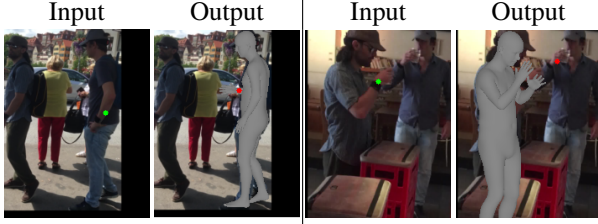


Figure 6: The right wrist is occluded in the first input image, making both Openpose and SPIN models misestimate the right wrist’s position. However, these wrong estimations are adjacent. The green dot shows the ground truth position, and the red dot represents the OpenPose estimation of the right wrist. In the second case, OpenPose is confused by the other person’s right wrist and makes a wrong estimation, while the SPIN model accurately estimates the right wrist. These are two samples that negatively affect the correlation between ED and SE.

when the models’ estimated positions are inaccurate, we expect the joint position estimations to be dissimilar. Hence, the distance between the models’ outputs

$$ED_i = \|x_i^{\text{SPIN}} - x_i^{\text{OP}}\|, \quad (5)$$

can be considered as a proxy for the confidence in the recovered human body mesh. Here x_i^{OP} are 2D joint estimates for OpenPose and x_i^{SPIN} are *projected* 2D joint estimates for SPIN. $ED_i \in \mathbb{R}^K$ and i refers to the image.

To investigate the hypothesis that ED is a useful proxy for the confidence in the recovered mesh, we calculate the correlation between the ED and the SPIN model’s error

$$SE_i = \|x_i^{\text{SPIN}} - x_i^{\text{gt}}\|. \quad (6)$$

The Pearson correlation coefficient of joint k which is shown by r_k is calculated using

$$r_k = \text{Corr}([ED_{0,k}, \dots, ED_{n,k}], [SE_{0,k}, \dots, SE_{n,k}]), \quad (7)$$

where n stands for the number of images in the dataset. Since the OpenPose model provides 2D estimates, it can only be compared to the 2D projection of the SPIN model output. Hence, SE only captures the 2D error of the SPIN model. Additionally, the OpenPose model does not provide any estimations for the undetected joints, which forces us to ignore those points for calculating the correlation. The computed correlation coefficient for the 3DPW test dataset for each joint is presented in Figure 5. The average coefficient $\bar{r} = 0.67$ indicates a strong correlation between ED and SE. This suggests that the differences in the estimated joint positions by SPIN and OpenPose models capture the error of SPIN model with respect to the ground truth. We leverage this information and explore three techniques that use ED to estimate confidence for the recovered mesh.

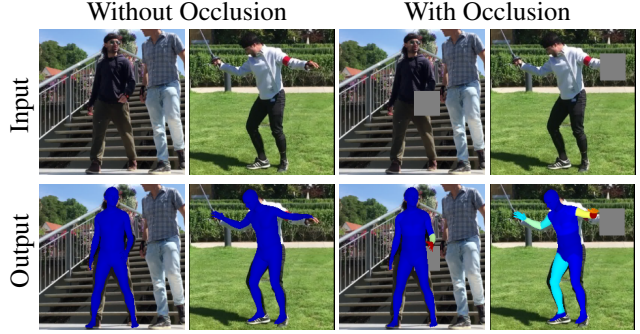


Figure 7: The error distribution on the estimated mesh changes when part of the human is occluded. For example, when a squared occluder is pasted onto the left hand, the model successfully identifies that is the least reliable region of the mesh (red regions on the mesh).

4.1. Using Raw ED Values

For a given image, ED is a K -dimensional vector that stores the differences between joints’ location estimates from SPIN and OpenPose models. We can use these values to decide whether or not the mesh is “good” as follows

$$y_{\text{mesh}} = \begin{cases} \text{good} & \text{if } \max ED \leq \text{threshold} \\ \text{bad} & \text{otherwise.} \end{cases} \quad (8)$$

We can use a similar argument to identify the worst joint:

$$k_{\text{worst}} = \arg \max_k ED. \quad (9)$$

4.2. Using Linear Regression

Plots shown in Figure 5 suggest a positive correlation between SE and ED (for all 14 joints), which suggests that it is possible to estimate SE given ED for a given joint. We are interested in estimating SE, since it represents the true SPIN error as computed using ground truth data. We do not have ground truth data at inference time, so instead we estimate SE using ED, which we can easily compute using SPIN and OpenPose models. Therefore, we fit a linear regressor

$$SE_k = (m_k)(ED_k) + c_k \quad (10)$$

that predicts $SE_{.,k}$ given observation $ED_{.,k}$, where $k \in [1, K]$. Given a new image, 1) compute ED, 2) use the trained linear regressor in Eq. 10 to estimate $SE \in \mathbb{R}^K$, and 3) use the estimated SE to decide whether or not mesh is “good” or to identify “good” and “bad” joints using the approach discussed in the previous section. Just substitute SE in place of ED.

Dataset	PCC		Mesh		WJ-R1		WJ-R3	
	R	O	R	O	R	O	R	O
3DPW	0.67	0.735	79.2%	86.2%	42.2%	45.4%	70.6%	73.8%
3DOH	0.665	0.707	81.6%	88%	37.3%	40.5%	64.2%	66.8%
H36M-P1	0.492	0.545	71.9%	82.1%	42.4%	43.9%	76.4%	75.1%

Table 1: Model Evaluation. Pearson Coefficient Correlation (PCC), model accuracy in separating accurate and faulty meshes (Mesh), and model performance on detecting the least reliable joints, i.e., worst joints (WJ), are presented in this table. Model is allowed a single guess for Rank 1 (R1) and it is allowed three guesses for Rank 3 (R3).

4.3. Classifiers

The previous two approaches of using ED to classify recovered human body meshes and joints treat each joint separately. We now propose an approach that looks at all K joints simultaneously to classify the mesh and identify the worst joint. Specifically, we use two multi-linear perceptron networks that use ED to classify mesh and identify the worst joint, respectively.

The Mesh Classifier (MC) network is a binary classifier containing three hidden linear layers that contain 10, 8, and 6 neurons respectively with ReLU activation functions. Input to MC is ED and it outputs whether or not the recovered mesh is reliable, i.e., all parts of the human body are visible in the image. MC network is trained using binary cross-entropy. The ground truth data for training MC is constructed using SE scores—if $SE_{.,k} \geq \text{threshold}$ for any k then the mesh is deemed unreliable, where $SE_{.,k}$ is the SE score for joint k . Under this regime

$$y_{\text{mesh}} = f_{\text{MC}}(\text{ED}). \quad (11)$$

The Worst Joint Classifier (WJC) network is a K -class classification network. It comprises three hidden layers containing 28, 56 and 28 neurons, respectively. Hidden layers use ReLU activation functions. ED is fed into WJC, and WJC is trained using cross-entropy. The ground truth data for training WJC is constructed from SE. We simply encode SE using one-hot-encoded form with 1 at $\arg \max_k SE$ and 0 elsewhere. Using WJC,

$$k_{\text{worst}} = f_{\text{WJC}}(\text{ED}). \quad (12)$$

5. Experiments and Results

We use 3DPW [27] and Human3.6M [8] (S9 and S11) datasets for model training and testing. In addition, we use 3DOH [31] dataset for testing only. The threshold used in Section 4 is set at 10 mm, i.e., if the difference between an estimated joint location and the ground truth joint location is higher than 10 mm, the mesh recovered by the SPIN model is labelled inaccurate. We also created occluded versions of the three datasets where a randomly selected joint is occluded using a square occluder in each image.

Figure 5 (rows 1 and 3) shows scatter plots of SE vs ED for every joint for the unoccluded 3DPW dataset. These plots also show Pearson correlation coefficient for each joint, which suggests that ED is positively correlated with SE. This is good news, since in the absence of SE, which is not available at inference time, we can use ED to compute an error estimate for the recovered mesh. Consider the ED vs. SE plot for right-wrist joint in Figure 5 (first row, right most figure). The plot identifies four regions labelled (a), (b), (c) and (d). Points in the regions (a) and (d) have a negative effect on the correlation. Points in region (a) suggest that there are several situations where both models are inaccurate, but that they agree with each other. Thus, we conclude that when the OpenPose and SPIN estimates are close to each other, it does not necessarily mean that the recovered human mesh is accurate. Rather, it may be that joint estimates from both models are close to each other but far from the ground truth locations. Figure 6 (input/output pair on the left) depicts such a case. Here both models are in agreement with each other, however, both models fail to detect the right wrist due to self-occlusion and the presence of other people. Points in region (d) represent cases where although the estimated values of SPIN and OpenPose model are different, the SPIN model is accurate. In other words, in some cases, a measurable difference in OpenPose and SPIN outputs does not indicate an inaccurate mesh reconstruction by the SPIN model. The right input/output pair in Figure 6 shows an example of such a case. The SPIN model is successful in estimating the right wrist of the person, however, OpenPose model makes a mistake and selects the other person’s hand position as the correct location for the right wrist. Despite the points in regions (a) and (d), the average Pearson correlation coefficient for all joints is $\bar{r} = 0.67$, indicating a strong correlation between ED and SE for all the joints. This confirms our intuition that ED is a good proxy for SE.

We performed a similar analysis as shown in Figure 5 (rows 2 and 4) for occluded dataset, where a square occluder is pasted on a randomly selected joint. The average Pearson correlation coefficient obtained under these settings is $\bar{r} = 0.735$, which is even higher than the value computed for the unoccluded case. This suggests two things:



Figure 8: Qualitative Results. Input images are shown in the left column. The next two columns contain the mesh classifier output and the ground truth. Unreliable meshes are shown in light pink. The fourth column highlights the least reliable joints. Red regions on the mesh correspond to the least reliable joints. The last column shows the ground truth for the least reliable joints.

1) that the proposed model is robust to occlusions and 2) ED is even more positively correlated with SE. Table 1 shows the Pearson correlation coefficient for different test datasets, and it shows Pearson correlation coefficient is higher for occluded datasets. In addition, 3DPW and 3DOH datasets have higher coefficient values since these exhibit higher occlusion levels. Figure 7 illustrates two instances of the model’s behavior towards occlusion. Our model predicts that the recovered mesh is correct when there are no occlusions, however, the model correctly identifies the left wrist region of the recovered mesh to be unreliable when a square occluder is used to hide this joint in the input image.

We exploit the positive correlation between ED and SE to estimate the error in the human body mesh recovered by SPIN. The proposed method also highlights the least reliable region of the recovered mesh. Table 1 lists our model’s performance at identifying an inaccurate mesh. Additionally, this table also includes model’s performance at iden-

Datasets	Metric	ED	L. Regressor	Classifier	
3DPW	R	Mesh	71.2	75.3	79.2
		WJ-R1	27.8	38.2	42.2
		WJ-R3	61.5	68.8	70.6
	O	Mesh	82.7	81.2	86.2
		WJ-R1	30.7	42.17	45.4
		WJ-R3	65.5	72.2	73.8
3DOH	R	Mesh	80.8	82.9	81.6
		WJ-R1	22	30.4	37.3
		WJ-R3	54.5	70.2	64.2
	O	Mesh	88.6	88	88
		WJ-R1	22.5	31.7	40.5
		WJ-R3	55.2	67.5	66.8
H36M-P1	R	Mesh	66.5	67.8	71.9
		WJ-R1	17.8	29	42.4
		WJ-R3	58.6	66.5	76.4
	O	Mesh	79.9	78.2	82.1
		WJ-R1	22.9	36	43.9
		WJ-R3	64.1	69.5	75.1

Table 2: Ablation Study. Comparing the method that uses raw ED values (column 3), linear regressor (column 4), and classifier based method (column 5) for classifying unreliable meshes and identifying the least reliable joints. Mesh refers to mesh reliability classification results, WJ-R1 refers to the results for identifying the worst joint (least reliable) when a single guess is allowed, and WJ-R3 refers to results for identifying the worst joint in three guesses.

tifying the least reliable joint. There is no baseline, since, to the best of our knowledge, ours is the first attempt at performing error estimation for single-image human body mesh reconstruction scenarios. For example, while the model was never trained on 3DOH dataset, it is able to identify an inaccurate mesh with 88% accuracy. The model is also able to identify the least reliable joint 40.5% accuracy. This number jumps to 66.8% when the model is allowed three guesses for the least reliable joint. These numbers are considerably higher than randomly selecting the least reliable joint. A similar trend is visible for 3DPW and H36M-P1 datasets.

Consider Figure 8 that presents some qualitative results. The first four rows show cases where the proposed model performed correctly. Here MC denotes output from the mesh classifier and MC-GT denotes the ground truth. WJC highlights the least reliable joint(s) and WJC-GT shows the least reliable joint ground truth. The bottom two rows show failure cases. Here, while the model correctly predicts that the recovered mesh is unreliable, it is unable to identify the least reliable joint correctly. Figure 9 shows an application of our method on video data. Here the top row shows input frames, the second row shows whether or not the recovered



Figure 9: Application on Videos. The first row shows the input video frames. The second row shows mesh reliability classification results. Light pink indicates an unreliable mesh. The last row shows least reliable joints. Here the meshes are rotated by 90 degrees for better visualization. The red regions on the mesh highlight the least reliable joint.

mesh is reliable, and the last row includes a visualization of the least reliable joint. The meshes shown in the last row are rotated to better see the least reliable joints. Our model correctly handles self-occlusions (top three rows) and occlusions due to other objects in the scene (bottom three rows). Check the last row where the model correctly predicts that the left foot is the least reliable region of the recovered mesh since it is not visible in the image (it is occluded by the table). The decision to decide if the recovered mesh is “reliable” when only left foot is not visible in the image is application specific. For example, say a robot is simply navigating around this person then perhaps it is okay to deem the recovered mesh to be reliable. However, if this same robot is carrying out a task that involves the left foot of this person then it is best to consider this mesh unreliable.

5.1. Ablation Study

We now compare the performance of the three approaches discussed in Section 4. All three approaches leverage the positive correlation between ED and SE. Table 2 shows the results obtained for each approach on the three datasets in both unoccluded and occluded cases. The results confirm that the classifier-based approach that combines ED information from different joints outperforms the other two methods. Method that uses raw ED values posts the worst performance. What is interesting to note is that

using a classifier dramatically increases the performance of identifying the least reliable joint, both when the model is allowed a single guess and when it is allowed three guesses. This suggests that it is beneficial to consider *all* joints’ errors when selecting the least reliable joint. For mesh classification, however, the improvement obtained by using a classifier-based approach over using the method that relies on raw ED values is not nearly as significant.

6. Conclusion

This work develops a method for estimating the error in the human body meshes reconstructed by the SPIN model. The model is not only able to decide whether or not a mesh is unreliable, it is also able to highlight the least reliable, i.e., having the highest error, regions on the mesh. The proposed model uses the disagreement between joint location estimates between OpenPose and SPIN model to compute error values for the recovered mesh. Pearson correlation coefficient studies on 3DPW dataset show this disagreement is a good proxy for the “true” error. Evaluations on 3DPW, 3DPH, and H36M-P1 confirm that the model is able to estimate error in the SPIN based single-image human body mesh reconstructions in the presence of occlusions. Furthermore, it is able to correctly estimate the error in SPIN meshes even when OpenPose estimates are incorrect. The model is also able to identify the least reliable joints. The

ability to estimate the error in the recovered meshes is particularly important when these meshes are used in human-robot interaction scenarios. To the best of our knowledge, ours is the first method to estimate error in single-image 3D human body mesh reconstruction.

References

- [1] Federica Bogo, Angjoo Kanazawa, Christoph Lassner, Peter Gehler, Javier Romero, and Michael J Black. Keep it simple: Automatic estimation of 3d human pose and shape from a single image. In *European conference on computer vision*, pages 561–578. Springer, 2016.
- [2] Zhe Cao, Tomas Simon, Shih-En Wei, and Yaser Sheikh. Realtime multi-person 2d pose estimation using part affinity fields. In *Proceedings of the IEEE conference on computer vision and pattern recognition*, pages 7291–7299, 2017.
- [3] Yu Chen, Chunhua Shen, Xiu-Shen Wei, Lingqiao Liu, and Jian Yang. Adversarial poseNet: A structure-aware convolutional network for human pose estimation. In *Proceedings of the IEEE International Conference on Computer Vision*, pages 1212–1221, 2017.
- [4] Nikita Dvornik, Julien Mairal, and Cordelia Schmid. Modeling visual context is key to augmenting object detection datasets. In *Proceedings of the European Conference on Computer Vision (ECCV)*, pages 364–380, 2018.
- [5] Miniar Ben Gamra and Moulay A Akhloufi. A review of deep learning techniques for 2d and 3d human pose estimation. *Image and Vision Computing*, 114:104282, 2021.
- [6] Georgios Georgakis, Ren Li, Srikrishna Karanam, Terrence Chen, Jana Košecká, and Ziyang Wu. Hierarchical kinematic human mesh recovery. In *European Conference on Computer Vision*, pages 768–784. Springer, 2020.
- [7] Eldar Insafutdinov, Leonid Pishchulin, Bjoern Andres, Mykhaylo Andriluka, and Bernt Schiele. DeepCUT: A deeper, stronger, and faster multi-person pose estimation model. In *European conference on computer vision*, pages 34–50. Springer, 2016.
- [8] Catalin Ionescu, Dragos Papava, Vlad Olaru, and Cristian Sminchisescu. Human3.6m: Large scale datasets and predictive methods for 3d human sensing in natural environments. *IEEE transactions on pattern analysis and machine intelligence*, 36(7):1325–1339, 2013.
- [9] Angjoo Kanazawa, Michael J Black, David W Jacobs, and Jitendra Malik. End-to-end recovery of human shape and pose. In *Proceedings of the IEEE conference on computer vision and pattern recognition*, pages 7122–7131, 2018.
- [10] Lipeng Ke, Ming-Ching Chang, Honggang Qi, and Siwei Lyu. Multi-scale structure-aware network for human pose estimation. In *Proceedings of the European conference on computer vision (ECCV)*, pages 713–728, 2018.
- [11] Rawal Khirodkar, Shashank Tripathi, and Kris Kitani. Occluded human mesh recovery. In *Proceedings of the IEEE/CVF conference on computer vision and pattern recognition*, pages 1715–1725, 2022.
- [12] Muhammed Kocabas, Chun-Hao P Huang, Otmar Hilliges, and Michael J Black. Pare: Part attention regressor for 3d human body estimation. In *Proceedings of the IEEE/CVF International Conference on Computer Vision*, pages 11127–11137, 2021.
- [13] Nikos Kolotouros, Georgios Pavlakos, Michael J Black, and Kostas Daniilidis. Learning to reconstruct 3d human pose and shape via model-fitting in the loop. In *Proceedings of the IEEE/CVF International Conference on Computer Vision*, pages 2252–2261, 2019.
- [14] Christoph Lassner, Javier Romero, Martin Kiefel, Federica Bogo, Michael J Black, and Peter V Gehler. Unite the people: Closing the loop between 3d and 2d human representations. In *Proceedings of the IEEE conference on computer vision and pattern recognition*, pages 6050–6059, 2017.
- [15] Jiefeng Li, Chao Xu, Zhicun Chen, Siyuan Bian, Lixin Yang, and Cewu Lu. Hybrik: A hybrid analytical-neural inverse kinematics solution for 3d human pose and shape estimation. In *Proceedings of the IEEE/CVF Conference on Computer Vision and Pattern Recognition*, pages 3383–3393, 2021.
- [16] Hongyi Liu and Lihui Wang. Human motion prediction for human-robot collaboration. *Journal of Manufacturing Systems*, 44:287–294, 2017.
- [17] Diogo C Luvizon, Hedi Tabia, and David Picard. Human pose regression by combining indirect part detection and contextual information. *Computers & Graphics*, 85:15–22, 2019.
- [18] Angel Martínez-González, Michael Villamizar, Olivier Canévet, and Jean-Marc Odobez. Real-time convolutional networks for depth-based human pose estimation. In *2018 IEEE/RSJ International Conference on Intelligent Robots and Systems (IROS)*, pages 41–47. IEEE, 2018.
- [19] Mohamed Omran, Christoph Lassner, Gerard Pons-Moll, Peter Gehler, and Bernt Schiele. Neural body fitting: Unifying deep learning and model based human pose and shape estimation. In *2018 international conference on 3D vision (3DV)*, pages 484–494. IEEE, 2018.
- [20] Georgios Pavlakos, Luyang Zhu, XiaoWei Zhou, and Kostas Daniilidis. Learning to estimate 3d human pose and shape from a single color image. In *Proceedings of the IEEE conference on computer vision and pattern recognition*, pages 459–468, 2018.
- [21] Leonid Pishchulin, Eldar Insafutdinov, Siyu Tang, Bjoern Andres, Mykhaylo Andriluka, Peter V Gehler, and Bernt Schiele. DeepCUT: Joint subset partition and labeling for multi person pose estimation. In *Proceedings of the IEEE conference on computer vision and pattern recognition*, pages 4929–4937, 2016.
- [22] István Sáráandi, Timm Linder, Kai O Arras, and Bastian Leibe. How robust is 3d human pose estimation to occlusion? *arXiv preprint arXiv:1808.09316*, 2018.
- [23] Ke Sun, Cuiling Lan, Junliang Xing, Wenjun Zeng, Dong Liu, and Jingdong Wang. Human pose estimation using global and local normalization. In *Proceedings of the IEEE international conference on computer vision*, pages 5599–5607, 2017.
- [24] Xiao Sun, Jiaxiang Shang, Shuang Liang, and Yichen Wei. Compositional human pose regression. In *Proceedings of the IEEE International Conference on Computer Vision*, pages 2602–2611, 2017.

- [25] Yating Tian, Hongwen Zhang, Yebin Liu, and Limin Wang. Recovering 3d human mesh from monocular images: A survey. *arXiv preprint arXiv:2203.01923*, 2022.
- [26] Hsiao-Yu Tung, Hsiao-Wei Tung, Ersin Yumer, and Katerina Fragkiadaki. Self-supervised learning of motion capture. *Advances in Neural Information Processing Systems*, 30, 2017.
- [27] Timo Von Marcard, Roberto Henschel, Michael J Black, Bodo Rosenhahn, and Gerard Pons-Moll. Recovering accurate 3d human pose in the wild using imus and a moving camera. In *Proceedings of the European Conference on Computer Vision (ECCV)*, pages 601–617, 2018.
- [28] Andrei Zanfir, Elisabeta Marinoiu, and Cristian Sminchisescu. Monocular 3d pose and shape estimation of multiple people in natural scenes-the importance of multiple scene constraints. In *Proceedings of the IEEE Conference on Computer Vision and Pattern Recognition*, pages 2148–2157, 2018.
- [29] Matthew D Zeiler and Rob Fergus. Visualizing and understanding convolutional networks. In *European conference on computer vision*, pages 818–833. Springer, 2014.
- [30] Feng Zhang, Xiatian Zhu, Hanbin Dai, Mao Ye, and Ce Zhu. Distribution-aware coordinate representation for human pose estimation. In *Proceedings of the IEEE/CVF conference on computer vision and pattern recognition*, pages 7093–7102, 2020.
- [31] Tianshu Zhang, Buzhen Huang, and Yangang Wang. Object-occluded human shape and pose estimation from a single color image. In *Proceedings of the IEEE/CVF conference on computer vision and pattern recognition*, pages 7376–7385, 2020.
- [32] Zhun Zhong, Liang Zheng, Guoliang Kang, Shaozi Li, and Yi Yang. Random erasing data augmentation. In *Proceedings of the AAAI conference on artificial intelligence*, volume 34, pages 13001–13008, 2020.